Universiteit Antwerpen

This item is the archived peer-reviewed author-version of:

Spin polarization in monolayer MoS_2 in the presence of proximity-induced interactions

Reference:
Zhao X.N., Xu W., Xiao Y.M., Van Duppen Ben.- Spin polarization in monolayer MoS_2 in the presence of proximity-induced interactions
International journal of modern physics: C - ISSN 0129-1831 - 31:10(2020), 2050143
Full text (Publisher's DOI): https://doi.org/10.1142/S0129183120501430
To cite this reference: https://hdl.handle.net/10067/1736350151162165141

uantwerpen.be
Institutional repository IRUA

Spin textures of monolayer MoS_2 in the presence of proximity-induced interactions

X. N. Zhao[1,2], W. Xu[1,3,*] Y. M. Xiao[3], and B. Van Duppen[4]

[1] *Key Laboratory of Materials Physics, Institute of Solid State Physics, Chinese Academy of Sciences, Hefei 230031, China*

[2] *Chinese University of Science and Technology, Hefei 230026, China*

[3] *School of Physics and Astronomy and Yunnan Key Laboratory for Quantum Information, Yunnan University, Kunming 650091, China and*

[4] *Department of Physics, University of Antwerp, Antwerpen B-2020, Belgium*

(Dated: April 18, 2020)

Abstract

Monolayer MoS_2 layer laid on a substrate would process proximity-induced interactions such as Rashba effect and exchange interaction. We reveal theoretically how the exchange interaction lifts the valley degeneracy. The spin and vally splittings are shown by varying the effective Zeeman field in presence of Rashba effect. The dependence of in-plane spin orientation on the magnitude of exchange interaction is also examined. The proper effective Zeeman field strength combined with Rashba parameter can result in the maxima of in-plane spin orientation. We also investigate the effect of exchange interaction on the spin polarization. This work can be helpful to understand physical effects of monolayer MoS_2 in the electromagnetic field such as the optical Hall effect.

Keywords: ML MoS_2, proximity-induced exchange, Rashba effect, optical Hall effect spin orientation.

PACS numbers:

*Electronic address: wenxu_issp@aliyun.com

I. INTRODUCTION

The typical transition metal metal dichalcogenide (TMD) Monolayer MoS_2 (ML-MoS_2) has received a great interest these years for the applications in valleytronics due to the two inequivalent valleys [1–3]. The strong intrinsic spin-orbit interaction (SOC) and the absence of inversion symmetry in ML-MoS_2 lead to the spin spitting subbands in conduction and valance band, respectively. The spin spitting subbands have different spin signs at each valley due to time-reversal symmetry [4, 5]. The unique electronic structure in ML-MoS_2 allows the existence of Berry curvature [4, 6] and further provides the possibility of many valley-dependent physical effects such as valley Hall effect [7, 8] and valley-selective circular dichroism [9, 10]. ML-MoS_2 layer coupled with the dielectric or magnetic substrates can arise proximity-induced interaction such as Rashba effect and exchange interaction. Those interactions can brings some interesting physical phenomenons. Our previous research [11] shows that the Rashba SOC can induce in-plane spin texture and adjust the spin splitting of the conduction and valence bands in the far infrared to terahertz (THz) bandwidth. On the other hand, the exchange interaction can significantly lifts the valley degeneracy by breaking time-reversal symmetry [12–14] and further lead to the valley polarization [15, 16]. However, both the Rashba SOC and exchange interaction play important roles in affecting the electronic structure of ML-MoS_2.

In this paper, we aim to study the effect of Rashba SOC and exchange interaction on the basic physical properties of ML-MoS_2 such as band structure, spin orientation and spin polarization. The results in this paper can provide the foundation for realization of the physical phenomenons such as the intra-band optical Hall effect in the far infrared to terahertz (THz) bandwidth. The paper is organized as follows. The theoretical approaches developed in this study are presented in Section II. The obtained results are presented and discussed in Section III. In Section IV, the conclusion and remarks are summarized.

II. THEORETICAL APPROACH

A. Electronic band structure

A low-energy effective Hamiltonian (LEH) is considered which includes the effects of proximity-induced interactions such as Rashba effect and exchange interaction. The LEH is

composed of four parts [12],

$$H = H_0 + H_{soc} + H_{ex} + H_R, \tag{1}$$

where

$$H_0 = \left[A(\zeta k_x \hat{\sigma_x} + k_y \hat{\sigma_y}) + \frac{\Delta}{2}\hat{\sigma_z}\right] \otimes \hat{\sigma_0}, \tag{1a}$$

$$H_{SOC} = \zeta\left[\lambda_c \hat{\sigma_+} + \lambda_v \hat{\sigma_-}\right] \otimes \hat{s_z}, \tag{1b}$$

$$H_{ex} = -\left[B_c \hat{\sigma_+} + B_v \hat{\sigma_-}\right] \otimes \hat{s_z}, \tag{1c}$$

$$H_R = \lambda_R\left[\zeta \hat{\sigma_x} \otimes \hat{s_y} - \hat{\sigma_y} \otimes \hat{s_x}\right], \tag{1d}$$

which represent the contribution from orbital interaction, intrinsic SOC, proximity-induced exchange, and Rashba SOC, respectively. Here, $\mathbf{k} = (k_x, k_y)$ is the electron wavevector along the 2D-plane, $\zeta = \pm$ refers to the K (K′) valley, $A = at$ with a being the lattice parameter and t the hopping parameter. λ_c and λ_v are the the intrinsic SOC parameters. B_c and B_v are effective Zeeman fields experienced by an electron in the presence of exchange coupling with the substrate. Δ is the direct band gap and λ_R is strength of Rashba SOC. Furthermore, the Pauli matrices $\hat{s_\alpha}$ and $\hat{\sigma_\alpha}$ refer to the real spin and orbital pseudospins where $\alpha = (x, y, z)$. $\hat{\sigma_0}$ is an unit 2×2 matrix and $\hat{\sigma_\pm} = (\hat{\sigma_0} \pm \hat{\sigma_z})/2$.

The corresponding eigenfunctions for electronic state near the K (K′) points are

$$|\mathbf{k}; \lambda >= \mathcal{A}[c_1, c_2, c_3, c_4]e^{i\mathbf{k}\cdot\mathbf{r}}, \tag{2}$$

where $\lambda = (\beta, \zeta, s)$ with $\beta = (c, v)$ referring to conduction or valence band. $\mathcal{A}$ is the normalization coefficient and $s = \pm$ indicates the spin-split bands, and

$$c_1 = -2i\lambda_R A^2 k_\zeta^{-2}, \qquad c_2 = A k_\zeta^- h_1,$$
$$c_3 = -2i\lambda_R A k_\zeta^- h_0, \qquad c_4 = h_2.$$

Here, $h_0 = E - \Delta/2 - d_\zeta^c$, $h_1 = (E - \Delta/2 - d_\zeta^c)(E + \Delta/2 - d_\zeta^v) - A^2k^2$, $h_2 = (E - \Delta/2 + d_\zeta^c)h_1 - 4\lambda_R^2 h_0$, and $d_\zeta^\beta = \lambda_\beta - \zeta B_\beta$.

B. In-plane spin orientation

With the electron wavefunction, one can examine the spin orientation of the electronic system. The spin orientation along different directions can be calculated through [17]

$$O_\alpha =< \tau, \mathbf{k}|\sigma_0 \otimes s_\alpha|\mathbf{k}, \tau > . \tag{3}$$

The in-plan spin orientation are

$$O_x = \frac{c_1c_2^* + c_2c_1^* + c_3c_4^* + c_4c_3^*}{\mathcal{A}^2} = -P_\zeta^{\beta,s}(k)\sin\theta, \tag{3a}$$

$$O_y = i\frac{c_1c_2^* - c_2c_1^* + c_3c_1^* - c_4c_3^*}{\mathcal{A}^2} = \zeta P_\zeta^{\beta,s}(k)\cos\theta, \tag{3b}$$

with θ being the angle between $\mathbf{k}$ and the x-axis, $P_\zeta^{\beta,s}(k) = 4\lambda_R Ak(A^2k^2h_0 + h_1h_2)/\mathcal{A}^2$. Eq. (3) indicates that the in-plane spin of electrons in ML-TMDs is induced by the Rashba SOC and it vanishes when $\lambda_R = 0$. Apparently, we can obtained that $[O_x(\mathbf{k})]^2 + [O_y(\mathbf{k})]^2 = |P_\zeta^{\beta,s}(k)|^2$ and $|P_\zeta^{\beta,s}(k)|$ is the magnitude of the in-plane spin orientation.

C. Spin polarization

Applying the condition of electron number conservation, the Fermi energy (or chemical potential) for electrons in n-type and holes in p-type ML MoS_2 is determined respectively by

$$n_e = \sum_{\mathbf{k},\zeta,s} f(E_c^{\zeta,s}(\mathbf{k})), \tag{4a}$$

$$n_h = \sum_{\mathbf{k},\zeta,s} [1 - f(E_v^{\zeta,s}(\mathbf{k}))], \tag{4b}$$

where $f(x) = [1 + \exp((x - E_F)/k_BT)]^{-1}$ is the Fermi-Dirac function with E_F being the Fermi energy or chemical potential, and $E_\beta^{\zeta,s}$ is the energy of spin-split subband in the two valleys. Thus, the in-plane spin polarization is given by

$$\mathcal{S} = \frac{(n_+^+ + n_+^-) - (n_-^+ + n_-^-)}{n_{e/h}}, \tag{4}$$

with n_ζ^s being the electron/hole density for spin-split conduction/valence bands in different valleys. When $\mathcal{S} \neq 0$, the electronic system is spin-polarized.

III. RESULTS AND DISCUSSIONS

For our numerical calculations in this study, we take the basic material parameters for ML-MoS_2 as given in Ref. [18–20] with $A = 3.5123$ ÅeV, $\Delta = 1.66$ eV , $2\lambda_c = 3$ meV, and $2\lambda_v = 150$ meV. The Rashba effect can be tuned through a gate voltage and a large Rashba parameter 72 meV was found in ML-$MoTe_2$ placed on a EuO substrate [12]. By the way, the

effective Zeeman field can also be tuned by manipulating the magnetization of substrates [13]. It has been shown theoretically that B_c and B_v can be as large as 206 meV and 170 meV when 2D TMD film is placed on EuO substrate [12]. In this study, we focus on the contributions from the effective Zeeman field. Thus, we take a fixed value of $\lambda_R = 70$ meV and B_c and B_v are as variable input parameters in our calculations.

In Fig. 1 we show the low-energy electronic band structure of ML-MoS_2 in present of proximity-induced interactions. In Fig. 1(a) where only the Rashba effect acts, we can see that a large Rashba parameter simply increases the spin splitting in conduction bands and decreases the spin splitting in valence bands. This is in line with the results in Ref. [11]. We take $\Delta E_{spin}^{\beta,\zeta}$ to quantify the spin splittings of conduction bands ($\beta = c$) and valence bands ($\beta = v$) at the two different valleys ($\zeta = \pm$). It is obvious that the spin splittings in two valleys are the same because energy spectra remains symmetric for the two valleys. After we take into account the exchange interaction with $B_c = 200$ meV and $B_v = 150$ meV, the corresponding band structure are shown in Fig. 1(b). Apparently, the symmetry is broken and the exchange interaction can significantly lift the valley degeneracy. The valley splitting at K(K′) point is quantified by the magnitude of $\Delta E_{val}^{\beta,s}$ which represents the energy spacing between the subbands with the same spin signs in different valleys as shown in Fig. 1(b).

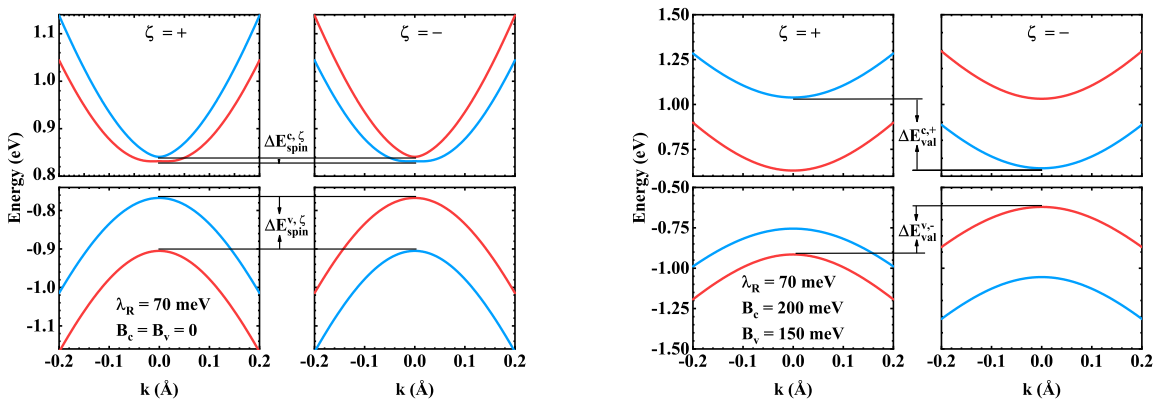

(a) (b)

FIG. 1: The conduction (upper panels) and valence (lower panels) band structure at the two valleys ($\zeta = \pm$) in ML MoS_2. The spin up/down states are represented by blue/red curves. (a) The results obtained by considering only the Rashba effect with $\lambda_R = 70$ meV, and (b) The results obtained by adding the proximity-induced exchange with $B_c = 200$ meV and $B_v = 150$ meV.

In Fig. 2 we show the energy of spin-spit subbands at K(K′) point for two valleys

($\zeta = \pm, s = \pm$) as a function of the effective Zeeman field. It is necessary to point out that B_c and B_v represent the effective Zeeman fields for the conduction and valence bands, respectively. For example, B_c with a strength of 200 meV can lift about 200 meV of energy splitting for conduction bands while less than 2 meV for valence bands. Thus, the effect of B_c on valence bands is negligible compared with that of on conduction bands. Apparently, it is the same with B_v. Therefore, we set $B_v = 0$ when we focus on the valence bands and set $B_v = 0$ when mainly consider the conduction bands. We can find from Fig. 2 that: (i) the minimum of $(+,+)$ and $(-,-)$ subbands or the minimum of $(-,+)$ and $(+,-)$ subbands are the same when $B_c = 0$ which indicates the energy symmetry at K and K′ valleys under the Rashba effect.

The energy spacing between $(+,+)$ and $(-,-)$ curves or $(-,+)$ and $(+,-)$ curves is the spin splitting induced by intrinsic SOC together with Rashba effect. and we set it as ΔE^0_β. (ii) For conduction bands the spin splitting $\Delta E^{c,+}_{spin}$ increase with B_c at $\zeta = +$ valley (the gap between the blue and yellow curves in Fig. 2(a)), while at $\zeta = -$ the $\Delta E^{c,-}_{spin}$ first decrease to 0 and then increase with B_c (the gap between the red and green curve in Fig. 2(a)); For valence bands the situation is just opposite in the opposite valley. However, the relative size of $E^{\zeta,s}_\beta(0)$ of the four conduction or valence subbands do not change with B_β (iii) The crossover of $(-,-)$ and $(-,+)$ conduction subbands or $(+,-)$ and $(+,+)$ subbands in valence subbands indicates that the proximity-induced exchange completely cancel out the effects of the intrinsic SOC and Rashba SOC on spin splitting. Due to the small ΔE^0_c of conduction bands the crossover is around $B_c = 5$ meV, and the crossover is around $B_v = 70$ because of the large ΔE^0_v. (iv) Regardless of the rise or the fall of the cures, the variation rate is always about B_β. Thus when $B_c < 5$ meV and $B_v < 70$ respectively, the valley splitting $\Delta E^{\beta,s}_{val} \simeq \Delta E^0_\beta$, and $\Delta E^{\beta,s}_{val} \simeq 2B_\beta$ when $B_c \geqslant 5$ and $B_v \geqslant 70$ (see the gap between the blue and green curves or the red and yellow curves).

We have know that Rashba SOC for hybridizes the valance and conduction bands and mixing the spin components so that spin possesses in-plane components [21, 22]. From Eq. (3) we demonstrate that the in-plane spin orientations of subbands with different up-down spin signs are in opposite direction and this result does not change with the parameter of Rashba effect and the proximity-induced exchange as long as the Rashba SOC exists. Also the strength of the in-plane spin orientations for conduction or valence subbands with different up-down spin signs in a certain valley is nearly equal. However we note that the

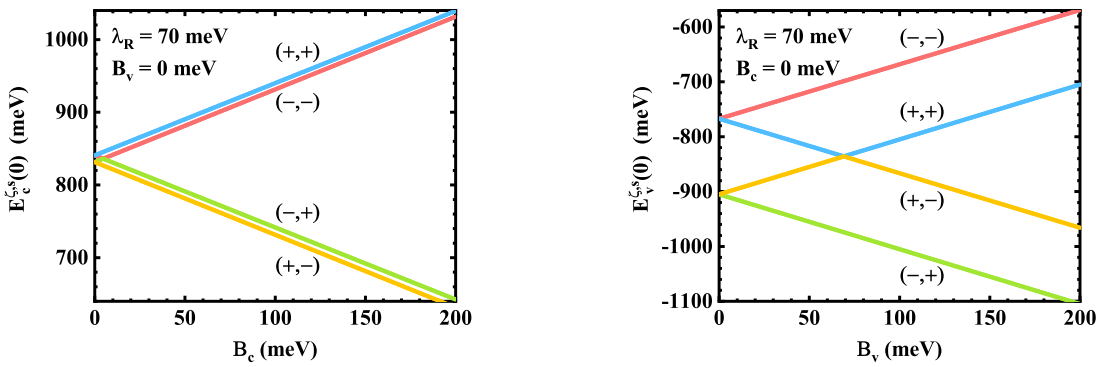

(a) (b)

FIG. 2: (a) The minima of four conduction subbands ($\zeta = \pm, s = \pm$) as a function of B_c for fixed values of $\lambda = 70$ meV and $B_v = 0$ meV. (b) The minima of four valence subbands ($\zeta = \pm, s = \pm$) as a function of B_v for fixed values of $\lambda = 70$ meV and $B_c = 0$ meV.

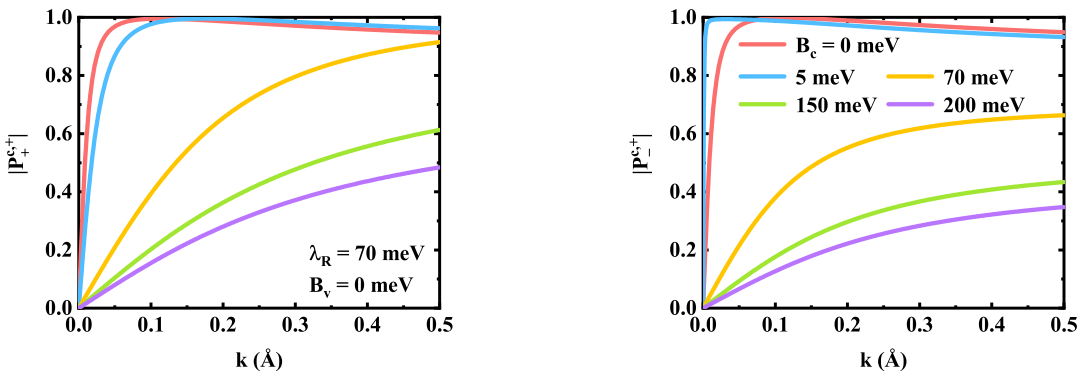

(a) (b)

FIG. 3: The size of in-plane spin orientation of spin-up conduction subband as a function of electron wavevector at fixed $\lambda_R = 70$ meV and $B_v = 0$ meV for different B_c for the K valley in (a) and K' valley in (b).

strength of the in-plane spin orientation, i.e. $|P_\zeta^{\beta,s}(k)|$, is valley dependent and also relates to the proximity-induced exchange. So in Figs. 3-4 we plot $|P_\zeta(k)|$ of spin-up conduction and valence subbands respectively in different valleys at different $B_{c/v}$. In general, the size of in-plane spin orientation for the K valley is lager than that for the K' valley at the same wave vector in both conduction and valence bands. That is because the energy gap between conduction band and valence band is smaller in K valley and the Rashba SOC

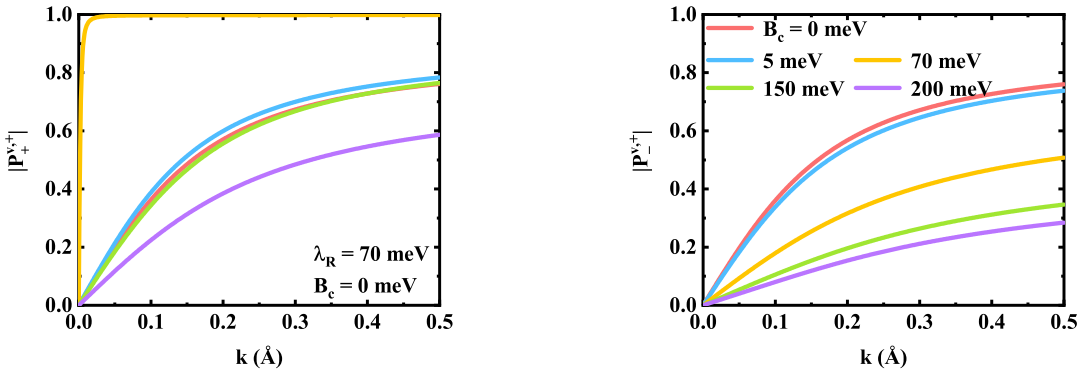

(a) (b)

FIG. 4: The size of in-plane spin orientation of spin-up valence subband as a function of electron wavevector at fixed $\lambda_R = 70$ meV and $B_c = 0$ meV for different B_v for the K valley in (a) and K' valley in (b).

can better hybridizes the valance and conduction bands. Also, the size of in-plane spin orientation generally decreases with increasing effective Zeeman field. However, we find two abnormal curves, the blue curve in Fig. 3(b) and the yellow curve in Fig. 4(a), show the largest in-plane spin orientation in conduction and valence bands respectively. Interestingly, the corresponding effective Zeeman fields are just $B_c = 5$ meV for conduction bands and $B_v = 70$ meV for valence bands and the corresponding spin splittings are nearly zero from Fig. 2. So we conclude that the proximity-induced exchange generally weaken the in-plane spin orientation, but we can have the strongest in one certain valley by tuning the Rashba parameter and the effective Zeeman field to obtain the energy degeneracy in one valley.

The spin polarizability $\mathcal{S}$ defined by Eq. (4) is shown in Fig. 5 as a function of total carrier density for different effective Zeeman fields at $T = 4.2$ K. First without proximity-induced exchange, time-reversal symmetry remains under the Rashba effect and the spin polarizability is constantly zero (see the red curve). When exchange interaction is present, the spin-split subbands with valley and spin index (ζ, s) are arranged from lower to higher energy as $(+,-)$, $(-,-)$, $(+,+)$ and $(+,-)$ for conduction bands in a n-type MoS_2 and as $(-,+)$, $(+,-)$, $(+,+)$ and $(-,-)$ for conduction bands in a p-type MoS_2 as given in Fig. 2. When the lowest conduction subband $(+,-)$ and the highest valence subband $(-,-)$ is occupied by electrons and holes respectively, the system is fully spin polarized. With the increasing carrier density, the spin polarization sharply decrease until a kink-like increase,

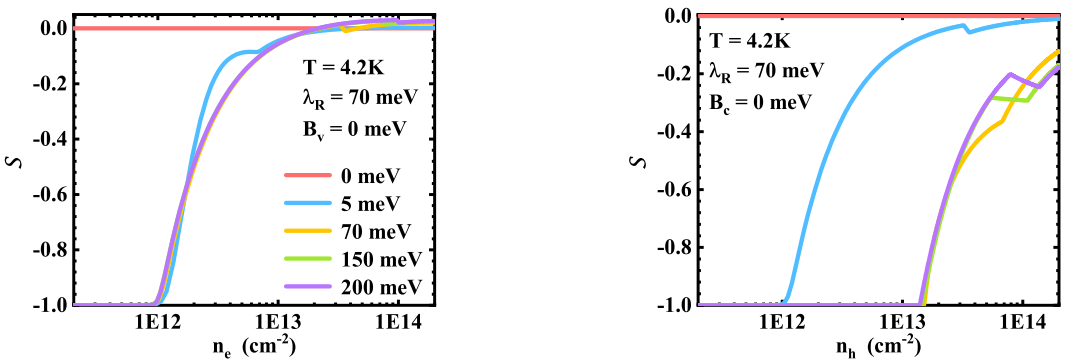

(a) (b)

FIG. 5: The spin polarizability $\mathcal{S}$ as a function of total electron density in (a) and hole density in (b) for different effective Zeeman field B_c and B_v respectively for fixed $\lambda_R = 70$ meV. The results are obtained at $T = 4.2$ K.

where the third subband is occupied by carriers, i.e., $(+,+)$ conduction subband and $(-,+)$ valence subband. And eventually the spin polarization decreases to nearly zero with a large carrier density. Specially at $B_c = 5$ meV for conduction bands and $B_v = 70$ meV for valence bands, the spin polarization does not show obvious kink-like increase, because the energy of $(-,-)$ and $(-,+)$ conduction subbands and $(+,+)$ and $(+,-)$ valence subbands is degenerate as shown in Fig. 2, and the two conduction/valence subbands are occupied by electrons/holes simultaneously. What's more, we find that the spin polarization is slightly affected by the effective Zeeman field. While before the turning point where $B_c = 5$ meV or $B_v = 70$ meV, we can assume that the Rashba SOC takes the dominant effect and the spin polarization is much larger at the same carrier density in this situation (see the blue curve in Fig. 5(b)). Thus we propose that it is better to tune the spin polarization by varing the Rashba parameter.

IV. CONCLUSIONS

In conclusion, we theoretically exam the co-effects of proximity-induced Rashba effect and exchange interaction on band structure, spin orientation and spin polarization of ML-MoS_2 on a substrate. We find that in the presence of Rashba SOC, the exchange interaction can lift the valley degeneracy only when the effective Zeeman field is larger than a certain turning

point in the corresponding valley. Before the turning point the Rashba effect take dominant, and after the turning point the exchange interaction come into prominence. The exchange interaction generally decreases the in-plane spin orientation, but the largest in-plane spin can be obtained at the turning point in the valley. Moreover, the spin polarization is slightly affected by the exchange interaction, while much larger spin polarization can be found when the effective Zeeman field is smaller than the turning point.

Acknowledgements

This work was also supported by the Ministry of Science and Technology of China (Grant No. 2011YQ130018), Department of Science and Technology of Yunnan Province, and by the Chinese Academy of Sciences.

---

[1] T. Cao, G. Wang, W. Han, H. Ye, C. Zhu, J. Shi, Q. Niu, P. H. Tan, E. Wang, B. L. Liu, and J. Feng, Nat. Commun. **3**, 887 (2012).

[2] J. R. Schaibley, H. Yu, G. Clark, P. Rivera, J. S. Ross, K. L. Seyler, W. Yao, and X. D. Xu, Nat. Rev. Mater. **1**, 16055 (2016).

[3] K. F. Mak and J. Shan, Nat. Photonics **10**, 216 (2016).

[4] D. Xiao, G. B. Liu, W. Feng, X. Xu, and W. Yao, Phys. Rev. Lett. **108**, 196802 (2012).

[5] J. F. Sun and F. Cheng, J. Appl. Phys. **115**, 1337032014)

[6] D. Xiao, W. Yao, and Q. Niu, Phys. Rev. Lett. **99**, 236809 (2007).

[7] G. Plechinger, T. Korn, and J. M. Lupton, J. Phys. Chem. **C 121**, 6409 (2017).

[8] N. Ubrig, S. Jo, M. Philippi, D. Costanzo, H. Berger, A. B. Kuzmenko, and A. F. Morpurgo, Nano. Lett. **17**, 5719 (2017).

[9] Y. J. Wu, C. Shen, Q. H. Tan, J. Shi, X. F. Liu, Z. H. Wu, J. Zhang, P. H. Tan, and H. Z. Zheng, Appl. Phys. Lett. **112**, 153105 (2018)

[10] Y. Z. Peng, J. Chen, Y. Song, and Y. Li, Appl. Surf. Sci. **366**, 310 (2016)

[11] Y. M. Xiao, W. Xu, B. Van Duppen, and F. M. Peeters, Phys. Rev. **B 94**, 155432 (2016).

[12] J. Qi, X. Li, Q. Niu, and J. Feng, Phys. Rev. **B 92**, 121403 (2015).

[13] C. Zhao, T. Norden, P. Zhang, P. Zhao, Y. C. Cheng, F. Sun, J. P. Parry, P. Taheri, J. Q.

Wang, Y. H. Yang, and T. Scrace, Nat. Nanotech. **12**, 757 (2017).

[14] C. Zhao, T. Scrace, P. Taher, P. Y. Zhang, T. Norden, B. Blizzard, A. Petrou, H. Zeng, P. Q. Zhao, and G. Kioseoglou, *APS Meeting*, Baltimore, Maryland, **61**, 2 (2016).

[15] K. F. Mak , K. L. He, Shan J, and T. F. Heinz, Nat. Nanotech. **7**, 494 (2012).

[16] H. L. Zeng, J. F. Dai, W. Yao, D. Xiao, and X. D. Cui, Nat. Nanotech. **7**, 490 (2012).

[17] E. I. Rashba, Phys. Rev. **B 79**, 161409 (R) (2009).

[18] Z. Y. Zhu, Y. C. Cheng, and U. Schwingenschlögl, Phys. Rev. **B 84**, 153402 (2011).

[19] H. Z. Lu, W. Yao, D. Xiao, and S. Q. Shen, Phys. Rev. Lett. **110**, 016806 (2013).

[20] Z. Li and J. P. Carbotte, Phys. Rev. **B 86**, 205425 (2012).

[21] H. Ochoa and R. Roldán, Phys. Rev. **B 87**, 245421 (2013).

[22] J. Klinovaja and D. Loss, Phys. Rev. **B 88**, 075404 (2013).